Journal of Alloys and Compounds 696 (2017) 820–827

Contents lists available at ScienceDirect

Journal of Alloys and Compounds

journal homepage: http://www.elsevier.com/locate/jalcom

Photoluminescence of single-phased white light emission materials based on simultaneous Tb^{3+}, Eu^{3+} and Dy^{3+} doping in $CaWO_4$ matrix

Helliomar P. Barbosa [a], Ivan G.N. Silva [a], Maria Claudia F.C. Felinto [b], Ercules E.S. Teotonio [c], Oscar L. Malta [d], Hermi F. Brito [a, *]

[a] Department of Fundamental Chemistry, Institute of Chemistry, University of São Paulo, 05508-000, São Paulo, SP, Brazil
[b] Nuclear and Energy Research Institute (IPEN-CQMA), 05508-000, São Paulo, SP, Brazil
[c] Department of Chemistry, Federal University of Paraiba, 58051-970, João Pessoa, PB, Brazil
[d] Department of Fundamental Chemistry, Federal University of Pernambuco, 50670-901, Recife, PE, Brazil

ARTICLE INFO

Article history:
Received 4 October 2016
Received in revised form
24 November 2016
Accepted 26 November 2016
Available online 27 November 2016

Keywords:
Rare earth
Alkaline earth tungstate
Charge transfer
White LEDs

ABSTRACT

The triply-doped $xTb^{3+}/xEu^{3+}/xDy^{3+}$ $CaWO_4$ (x: 0.5, 1.0, 2.0, 3.0, 4.0 and 5.0 mol%) nanomaterials were prepared at room temperature by a coprecipitation method. The luminescence materials were characterized by X-ray powder diffraction (XPD), thermal analysis (TG), infrared absorption spectroscopy (FTIR) and UV excited photoluminescence. The prepared powder phosphors are single-phase scheelite structure with porous morphology and particle sizes around 11 nm. The materials display white color from cool to the warm white, under UV excitation, as a result of the intraconfigurational 4f transitions from trivalent rare earth ions. The non-radiative energy transfer processes from the O→W and O→Eu LMCT as well as the $4f^8 \rightarrow 4f^7 5d^1$ states to the intraconfigurational 4f excited levels of rare earth ions and simultaneous emissions from the $^4F_{9/2}$ (Dy^{3+})→$^5D_4$ (Tb^{3+})→$^5D_1$,$^5D_0$ (Eu^{3+}) emitter levels are reported. Furthermore, CIE parameters and the color correlated temperature (CCT) are discussed in order to characterize the color emission. Based on the results, these luminescence materials may be potential candidates for white light emitting diodes and solid-state lighting.

1. Introduction

Nowadays, there is an increasing attention to the development of white emitting materials applied to the light-emitting diodes (LEDs) instead of conventional incandescent and fluorescent lamps. These luminescence materials exhibit new advantageous as power efficiency, energy saving, environmental friendliness, no mercury and extended operation time compared to the predominant incandescent and fluorescent lamps [1–5]. Usually, many luminophores applied in white-LEDs are based on two or three different phosphors consisting of the blue, green and red emission colors, exhibiting different thermal stability and degradation leading to a higher costs [5]. For example, the white light emitting phosphors can be reached by the combination of the blue LED chip GaN with YAG:Ce^{3+}, K_2SiF_6:Mn^{4+} and β-SiAlON:Eu^{2+} materials, showing the yellow, red and green emission colors, respectively [1]. However, the mixture of different phosphors can result in both low reproducibility and low Color Rendering Index (CRI). Another failing includes high Corrected Color Temperature (CCT > 7000 K) due to the lack of a red emission light component that limits its multiple applications [6,7].

These disadvantages can be overcome by using different activator ions in the same host matrix called the single-phase white light-emitting phosphor that is usually excited by UV radiation. This kind of luminescence materials has a great advantage such as high CRI, high luminescence efficiency and lower manufacturing cost that are excellent alternatives for applications in LEDs and in white-light-emitting diodes (WLEDs). Generally, the single-phase materials applied in WLEDs work as a result of non-radiative energy transfers (ET) from a sensitizer to activators as an efficient way to obtain a warm white light.

Currently, luminescence materials based on ET process such as $Sr_3B_2O_6$:Ce^{3+},Eu^{2+}, $Sr_3Gd_2(Si_3O_9)_2$:Ce^{3+},Tb^{3+}/Mn^{2+}, $Ca_9Mg(PO_4)_6F_2$: Eu^{2+},Mn^{2+} and $NaCaBO_3$:Ce^{3+}/Mn^{2+} have been used [8–11]. However, in preparation of these photonic materials, a reducing atmosphere and long reaction time is necessary, leading to a high cost and energy spent [12]. In the last years, were reported

* Corresponding author.
E-mail address: hefbrito@iq.usp.br (H.F. Brito).

http://dx.doi.org/10.1016/j.jallcom.2016.11.378
0925-8388/

single-doped tricolor emission phosphors in only one matrix containing rare earth ions (RE^{n+}) prepared by different synthetic routes like Ca_2SiO_4:RE (RE: Ce^{3+}, Eu^{2+}, Sm^{3+}) and $Ca_2Mg_{0.75}Al_{0.5}Si_{1.75}O_7$:$RE^{3+}$ (Ln: Ce^{3+}, Dy^{3+}, Eu^{3+}, Sm^{3+}) by the conventional solid-state method and $CaO-Al_2O_3-B_2O_3-RE_2O_3$ (RE: Eu^{3+}, Tb^{3+}, Tm^{3+}) prepared by melt quenching method [12–14].

The $CaWO_4$:RE^{3+} nanophosphors have demonstrated interesting luminescence properties with potential applications in several fields as waveguide lasers host materials, optical fibers, organic light-emitting diodes (OLEDs), photovoltaic devices, luminescent materials [15–19]. In addition, tungstate $[WO_4]^{2-}$ based matrices are an important family of phosphors due to their excellent thermal stability and interesting optical behavior [20–22]. The $CaWO_4$ can be doped and activated with NUV-blue light-absorbing ions for applications in WLEDs due the efficient energy transfer from tetragonal tungstate groups $[WO_4]^{2-}$ to the activator RE^{3+} ions [23–29]. Besides, the RE^{3+} doped in the MWO_4 matrices (M^{2+}: Ca, Sr, Ba) present $O^{2-}(2p) \rightarrow Eu^{3+}(4f)$, $O^{2-}(2p) \rightarrow W^{VI}(5d)$ Ligand–to–Metal Charge Transfer (LMCT) states and Tb^{3+} $4f^8 \rightarrow 4f^7 5d^1$ interconfigurational transitions as well as the RE^{3+} 4f-intraconfigurational transitions, which may to improve the luminescence efficiency of these materials. The design of the phosphors leading to the color tuning arising from the narrow line emission bands assigned to the 4f-4f transitions of RE^{3+} ions. It is important to point out that the Dy^{3+} ion may acts as a sensitizer and can partially transfer energy from the $^4F_{9/2}$ state to the $^5D_4$ and $^5D_0$ emitting levels of the Tb^{3+} and Eu^{3+} ions, respectively. In addition, the Tb^{3+} ion acts as a good sensitizer to Eu^{3+} activator transferring part of the energy from the $^5D_4$ level to the emitting $^5D_1$,$^5D_0$ level of Eu^{3+} ion [30,31]. The full-color single-phased phosphors arising from the combination of green (Tb^{3+}), yellow (Dy^{3+}) and red (Eu^{3+}) emission bands can potentially be used for high luminous efficient white LEDs [32].

The tungstate materials prepared by ceramic method need high temperatures (>1000 °C) and long reaction time and reducing atmosphere, leading to a high energy consumption as well as inhomogeneity of the material particles [33]. However, the coprecipitation method exhibits many benefits such as short reaction time, straightforward operation at room temperature. This procedure is environmental friendly producing materials with high crystallinity and controlled particle size [22,34].

In this work, the simultaneous incorporation of the Tb^{3+}/Eu^{3+}/Dy^{3+} triply-doped $CaWO_4$ matrix as a possible alternative to solid state synthesis is to use the “green procedure” applying a coprecipitation method as well as their luminescence properties are described. Moreover, the $[WO_4]^{2-}$ and Eu^{3+} LMCT states and $4f^8 \rightarrow 4f^7 5d^1$ (Tb^{3+}) transitions are also discussed. Finally, the non-energy transfer process from the tungstate host lattice to the rare earth ions as well as between their 4f-4f transitions of the $^4F_{9/2}$ (Dy^{3+}), $^5D_4$ (Tb^{3+}) and $^5D_1$ (Eu^{3+}) emitting levels are also analyzed and elucidated.

2. Experimental section

The RE^{3+} dopant ions were obtained from their respective oxides RE_2O_3 (Cstarm, 99.99%) for Eu^{3+} and Dy^{3+} and Tb_4O_7 (Cstarm, 99.99%) for Tb^{3+} by digestion of their aqueous suspensions with the addition of concentrated hydrochloric acid until pH reaches 6. The $RECl_3 \cdot 6H_2O$ resulted white crystalline solids were dried and filtered and afterwards stored under reduced pressure in vacuum desiccator. The $CaWO_4$:xTb^{3+},xEu^{3+},xDy^{3+} (x: 0.5–5.0 mol%) materials were prepared with conventional coprecipitation reaction using aqueous solution of Na_2WO_4 (99.99% Vetec), $CaCl_2$ (99.99% Alfa) and $RECl_3$. The RE^{3+} doping concentrations were identical for each rare earth ion in following concentrations: 0.5, 1.0, 2.0, 3.0, 4.0 and 5.0 mol% of the Ca^{2+} amount.

The $CaWO_4$:RE^{3+} (5.0 mol%) material was prepared from a mixture of $CaCl_2 \cdot 2H_2O$ (0.085 mol L^{-1}) and $RECl_3 \cdot 6H_2O$ aqueous solutions (RE^{3+}: Tb, Eu and Dy; 0.05 mol L^{-1}). After, the resulting solution was dropwise added into the $Na_2WO_4 \cdot 2H_2O$ (0.1 mol L^{-1}) aqueous solution under magnetic stirring, leading to white precipitate immediately. The crystalline powders were washed with distilled water for thrice, filtered and after dried under reduced pressure in vacuum desiccator. The as-prepared materials are air stable and non-hygroscopic. The synthesis of the materials at different doping RE^{3+} concentrations 0.5, 1.0, 2.0, 3.0 and 4.0 are similar to 5.0 mol% one.

The infrared absorption spectra were performed with KBr pellets with the equipment Bomem MB100 FTIR apparatus in the spectral region from 400 to 4000 cm^{-1}. The X-ray powder diffraction (XPD) patterns were registered by a Miniflex Rigaku (Cu $K_{\alpha 1}$ 1.5406 Å) from 5 to 60° (2θ) with the step of 0.02° and step integration time of 1 s.

The scanning electron microscopy (SEM) images and the energy dispersive spectroscopy (EDS) elemental mapping were obtained with a JEOL JSM-7401F Field Emission Scanning Electron Microscope with the acceleration voltages of 5 and 15 kV, respectively. For the SEM images, the solid samples were deposited on carbon graphite sample holder. In the EDS mapping, the samples were prepared by dispersing the materials in chloroform. The suspension was submitted to ultrasound for 15 min and then placed on a carbon graphite grid sample holder.

Thermogravimetric (TG) curves were obtained with the 2950 TGA HR V5.4A equipment from 40 to 950 °C in a dynamic atmosphere of synthetic air with constant heating rate of 10 °C min^{-1}. The photoluminescence study was conducted based on the excitation and emission spectra recorded at room temperature (300 K) by use of the front-face data collection mode (22.5°) with a 450 W Xenon lamp as the irradiation source coupled to the equipment SPEX-Fluorolog 2 with double monochromators. The luminescence decay curves were recorded with a 150 W pulsed xenon lamp attached to the SPEX 1934D phosphorimeter accessory. The CIE (*Commission Internationale de l'Eclairage*) color coordinates were calculated from the emission spectra by use of SpectraLux v2.0 software [35].

3. Results and discussion

The thermogravimetric curves of triply-doped $CaWO_4$:xTb^{3+},xEu^{3+},xDy^{3+} (x: 0.5–5.0 mol%) materials exhibit low weight loss event in the temperature interval from 40 to 800 °C, indicating good thermal stability of the materials (Fig. 1). The first weight loss (1.5%) event is observed between 40 and ~130 °C due to adsorbed/absorbed water, suggesting that the crystalline material has no phase impurities in its composition. The water loss corresponds to 0.25 mol H_2O of the $CaWO_4$:Tb^{3+},Eu^{3+},Dy^{3+} (5.0 mol%) material. It is expected the existence of hemihydrate form $WO_4 \cdot 0.5H_2O$ in the system, since the material contains high RE^{3+} doping concentration [36]. Due to the proximity, the rare earth ions can share the molecules of water resulting in a hemihydrate compound.

The infrared absorption spectra (FTIR) of the $CaWO_4$:Tb^{3+},Eu^{3+},Dy^{3+} (x mol%; x: 0.5–5.0) materials show medium absorption band at around 3400 cm^{-1} assigned to the O–H stretching vibrations owing to the adsorbed water by the KBr pellets and the compounds (Fig. S1). The intense absorption band located at 800 cm^{-1} is attributed to the W–O symmetric stretching mode and the absorption peak at 400 cm^{-1} are assigned to the δ (Ca–O) bending modes [22,37]. Besides, the undoped and doped materials present similar FTIR features despite the high doping

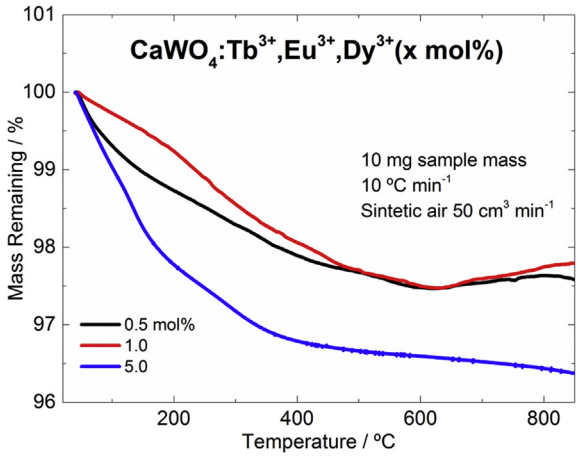

Fig. 1. Thermogravimetric curves of $CaWO_4$:xTb^{3+},xEu^{3+},xDy^{3+} (x: 0.5, 1.0 and 5.0 mol %) materials recorded in dynamic synthetic air atmosphere.

concentrations of the rare earth ions (Tb^{3+}, Eu^{3+} and Dy^{3+} from 0.5 to 5.0 mol%) in the phosphors.

The X-ray powder diffraction (XPD) patterns of the $CaWO_4$:Tb^{3+},Eu^{3+},Dy^{3+} materials suggest the tetragonal scheelite phase with the $I4_1/a$ space group (PDF entries: $CaWO_4$ 41-1431 strongest reflections at 2θ values of 18.58 [101] and 28.74 [112] (Fig. 2a) [38]. There are no additional diffraction peaks arising from the impurities or the $RE_2(WO_4)_3$ phase, confirming the successfully preparing of the $CaWO_4$:Tb^{3+},Eu^{3+},Dy^{3+} materials, even at higher

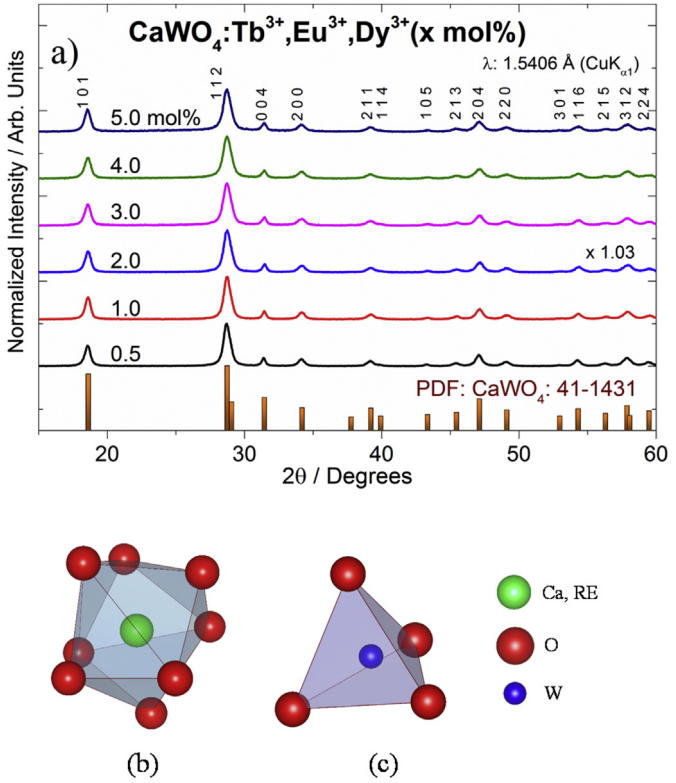

Fig. 2. a) The X-ray powder diffraction (XPD) patterns of the $CaWO_4$:xTb^{3+},xEu^{3+},xDy^{3+} (x: 0.5, 1.0, 2.0, 3.0, 4.0 and 5.0 mol%) materials. Vertical bars at the bottom of the figure indicate the standard PDF [ICDD entry #41-1431] [33] data for the tetragonal $CaWO_4$ phase. b) CaO_8 polyhedron distorted cube and c) WO_4 polyhedron exhibit in $CaWO_4$ nanoparticles.

doping concentrations. The XPD data indicate the efficient incorporation of rare earth ions into the $CaWO_4$ matrix owing to the similarity of 1.06, 1.04, 1.02 and 1.12 Å ionic radii of the Eu^{3+}, Tb^{3+}, Dy^{3+} and Ca^{2+} metal ions, respectively [39]. The ionic radii values obeys the Vegard's law that establishes a limit of around 15% to obtain complete solid solubility between the RE^{3+} ions that occupy the Ca^{2+} site in host lattice [39]. The RE^{3+} ions replace the Ca^{2+} with 8 oxygen atoms in the distorted dodecahedral sites [CaO_8] (Fig. 2b) and the tungsten ions [WO_4] are coordinated to four oxygens with the O–W–O angles slightly distorted from the tetrahedral ones of $CaWO_4$ scheelite (Fig. 2c) [40].

It is noteworthy that the incorporation of RE^{3+} ions into a $CaWO_4$ host lattice substitute a divalent metal ion (Ca^{2+}), charge balancing is required. The RE^{3+} ion replace one Ca^{2+} ion, but the ionic radii mismatch would make accommodation of RE^{3+} more difficult. Furthermore, in solution with excess of Na^+ (from Na_2WO_4), this ion goes into the $CaWO_4$:RE^{3+} lattice since the size of Na^+ (1.18 Å, CN: 8) is slightly larger than that of Ca^{2+} (1.12 Å, CN: 8). In these materials, two Ca^{2+} sites are substituted by trivalent rare earth ion and one Na^+ ion ensuring overall charge equilibrium compensating the charge mismatch [22].

The average crystallite sizes of the $CaWO_4$:xTb^{3+},xEu^{3+},xDy^{3+} materials (x: 0.5, 1.0, 2.0, 3.0, 4.0, 5.0 mol%) are 12.9, 12.8, 12.1, 10.8, 10.7, 11.5 nm, respectively (Fig. 3). The average crystallite sizes were estimated from the diffraction data by the Scherrer formula $D_{hkl} = 0.9\lambda/\beta\cos\theta$ [41]. Where D_{hkl} is the average grain size, λ the X-ray wavelength, θ half of the Bragg angle, and β is the full width at half maximum (FWHM) of the selected reflection. In this work, the [112] reflection (2θ: 28°) was used in the calculations. In order to correct the broadening due to the diffractometer setup from the β_s was used $\boldsymbol{\beta^2 = \beta_s^2 - \beta_r^2}$ where the β_s and β_r are the FWHM of the material and reference (NaCl: 0.149; 31.7°; hkl: [2 0 0]), respectively. The reduction in the crystallite size from 0.5 to 4.0 mol% (Fig. 3) is mainly due to the distortion in the host $CaWO_4$ lattice by the dopants (i.e., RE^{3+}), that can retard the crystal growth rate of $CaWO_4$ reaching a minimum when the doping concentration of each RE^{3+} ion is 4.0 mol% [42]. The XPD results confirm that the coprecipitation method produced materials with high crystallinity.

The fast precipitation process of $CaWO_4$ doped phosphors due to the attraction of Ca^{2+}, $[WO_4]^{2-}$ and RE^{3+} ions and subsequent bond between them can result in formation of defects, deformations, or strains in the crystal structure [38]. The microstrain can be calculated using Equation (1): [42].

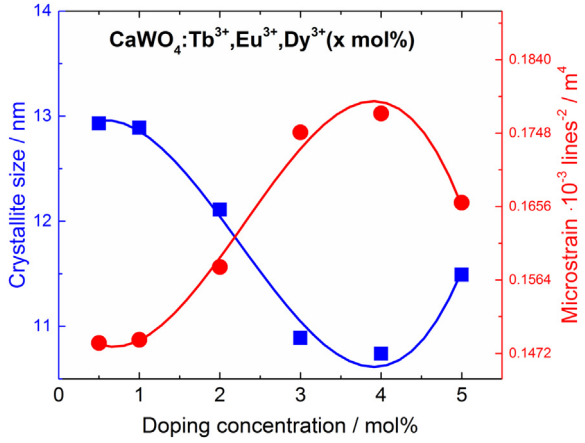

Fig. 3. Crystallite size and microstrain of the $CaWO_4$:xTb^{3+},xEu^{3+},xDy^{3+} (x: 0.5, 1.0, 2.0, 3.0, 4.0 and 5.0 mol%) materials according de doping concentration [36].

$$\varepsilon = \frac{\beta cos\theta}{4} \quad (1)$$

The microstrain values of the doped materials 0.148, 0.148, 0.159, 0.175, 0.177 and 0.166 (10^{-3}lines^{-2} m^{-4}) increase with decrease of crystallite size 12.9, 12.8, 12.1, 10.8, 10.7, 11.5 nm, respectively (Fig. 3). This effect is a consequence of the small distortion of CaO_8 dodecahedra up to 4.0 mol% RE^{3+} doping concentration. On the other hand, the phosphor with 5.0 mol% RE^{3+} doping concentration the crystallite size increases slightly and the microstrain decreases simultaneously. Although the material with RE^{3+} 5.0 mol% has shown a smaller microstrain value ($0.166 \cdot 10^{-3}$lines^{-2} m^{-4}; 11.5 nm) this can indicate the slightly increase of crystallinity of the material with this doping concentration due to reach for upper limits of the Vegard's law. In addition, the microstrain curve profile (Fig. 3) are corroborated to those reported for Gao et al. [42].

The scanning electron microscopy (SEM) and Energy-dispersive X-ray spectroscopy (EDX) images present the morphological features and composition of the $CaWO_4$:Tb^{3+},Eu^{3+},Dy^{3+} (5.0 mol%) phosphors (Fig. 4). The material with lower RE^{3+} doping concentration (0.5 mol%) exhibits a spherical micrometric particle with diameter around 4 μm. In addition, the increase of RE^{3+} doping concentration (5.0 mol%) has shown effect on the morphological features, disturbing the spherical shape.

The EDX mapping provides the chemical composition of the sample containing O, Ca, Eu, Tb, Dy and W and no other impurity can be detected. This clearly depicts the incorporation of rare earth ions and their distribution inside the spherical structure like "tennis ball form". Combined with above XPD patterns, confirm a homogeneous incorporation of rare earths ions in the $CaWO_4$ host lattice.

4. Photoluminescence properties

The excitation spectra of the $CaWO_4$:Tb^{3+},Eu^{3+},Dy^{3+} (x mol%; x: 0.5–5.0) materials recorded by monitoring the emission intensity of the $^5D_4 \rightarrow {}^7F_5$ transition (at 545 nm) of Tb^{3+} in the spectral range from 225 to 510 nm at room temperature showing similar spectral features (Fig. 5). It is observed absorption bands in the range of

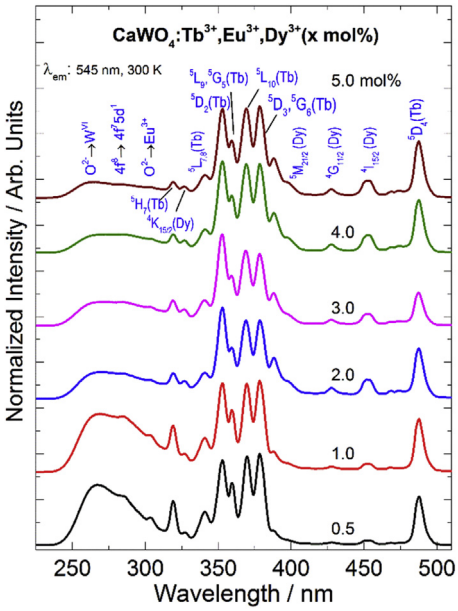

Fig. 5. Excitation spectra of the $CaWO_4$:xTb^{3+},xEu^{3+},xDy^{3+} (x: 0.5, 1.0, 2.0, 3.0, 4.0 and 5.0 mol%) materials recorded at room temperature monitoring the Tb^{3+} $^5D_4 \rightarrow {}^7F_5$, under emission at 545 nm.

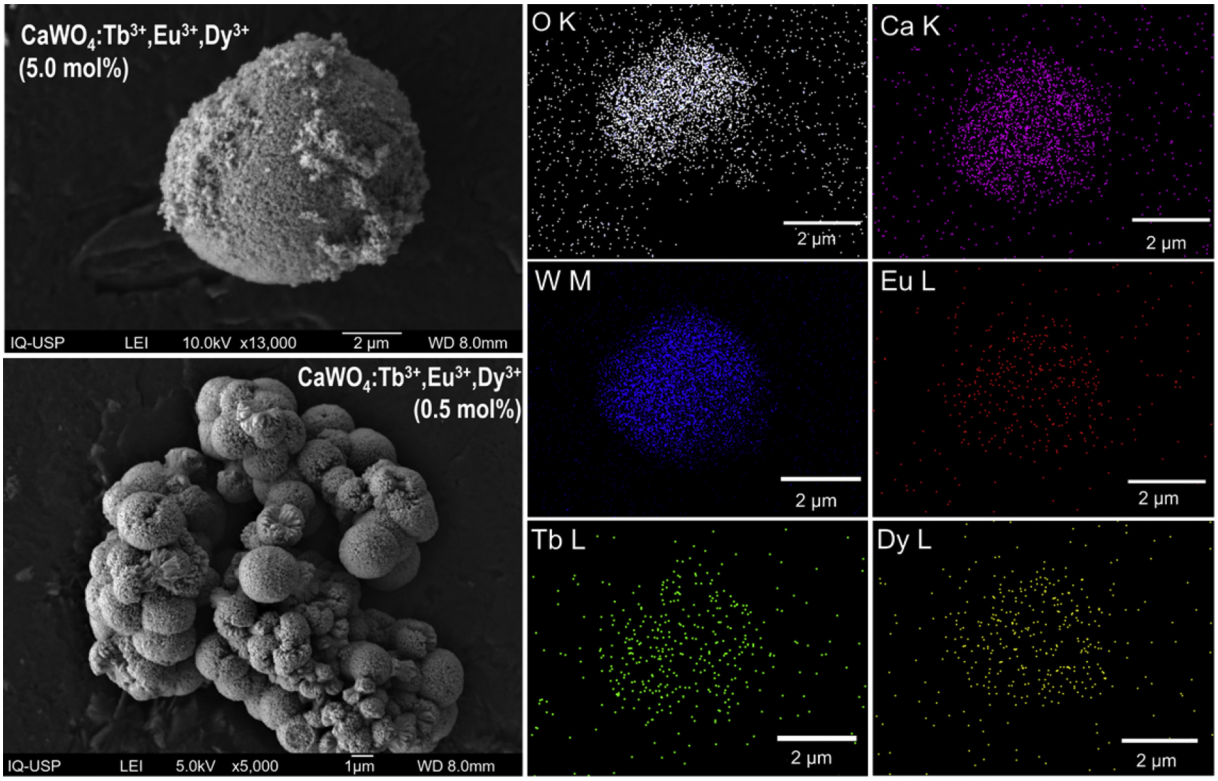

Fig. 4. FESEM of an individual tennis ball-like of $CaWO_4$:Tb^{3+},Eu^{3+},Dy^{3+} (5.0 mol%) material with elemental mapping of O, Ca, W, Eu, Tb and Dy. Agglomerate of spherically shape in lower doping concentration material.

220–320 nm, which are assigned to the O–W (~270 nm) and O→Eu (~310 nm) Ligand-to-Metal Charge Transfer (LMCT) states from the excited 2p orbitals of O^{2-} belong to the $[WO_4]^{2-}$ groups to the empty orbitals of the W^{VI} and Eu^{3+} ions, respectively. These bands are overlapped with that one the $4f^8 \rightarrow 4f^7 5d^1$ inter-configurational transition of the Tb^{3+} ion around 280 nm [43]. It is important to mention that the LMCT and $4f^8 \rightarrow 4f^7 5d^1$ transitions have broad absorption bands with high intensities because they involve parity-allowed electronic transitions to the outer 5d orbitals.

Excitation spectra also exhibit groups of narrow absorption bands assigned to the 4f intraconfigurational transitions (Fig. 5) from the ground states $^7F_6$ (Tb^{3+}) and $^6H_{15/2}$ (Dy^{3+}) to excited states in order of increasing energy as following (in cm^{-1}): 20,508 $^7F_6 \rightarrow {}^5D_4$($Tb^{3+}$), 21,159 $^6H_{15/2} \rightarrow {}^4F_{9/2}$($Dy^{3+}$), 22,099 $^6H_{15/2} \rightarrow {}^4I_{15/2}$($Dy^{3+}$), 23,339 $^6H_{15/2} \rightarrow {}^4G_{11/2}$($Dy^{3+}$), 26,399 $^7F_6 \rightarrow {}^5D_3$,$^5G_6$($Tb^{3+}$), 27,085 $^7F_6 \rightarrow {}^5L_{10}$($Tb^{3+}$), 27,824 $^7F_6 \rightarrow {}^5L_9$,$^5G_5$($Tb^{3+}$), 28,312 $^7F_6 \rightarrow {}^5D_2$, ($Tb^{3+}$), 29,308 $^7F_6 \rightarrow {}^5L_{7,8}$ (Tb^{3+}), 30,599 $^6H_{15/2} \rightarrow {}^4K_{15/2}$($Dy^{3+}$), 31,368 $^7F_6 \rightarrow {}^5H_7$($Tb^{3+}$), 32,852 $^7F_6 \rightarrow {}^5H_6$($Tb^{3+}$) and 35,088 $^7F_6 \rightarrow {}^5I_8$,$^5F_5$($Tb^{3+}$) [43,44].

Usually, the 4f – 4f transitions of the rare earth ions have low absorption and emission intensities due to their parity-forbidden by Laporte's rules ($\Delta l = \pm 1$), but this rule is slightly relaxed due to the mixing of opposite parity electronic configurations, produced by the odd components of a non-centrosymmetric ligand field [45]. It is noteworthy that the relative absorption intensities between from 4f intraconfigurational transitions and those ones arising from other kind of transitions decrease significantly with the increasing of the rare earth ions concentration indicating the cross relaxation process among rare earth ions.

Interestingly, Fig. 5 shows several narrow absorption bands from terbium and dysprosium ions when the excitation is monitored at 545 nm corresponding to the emission $^5D_4 \rightarrow {}^7F_5$ transition of Tb^{3+} ion. These spectroscopic data indicate that the non-radiative energy transfer occur from Dy^{3+} to Tb^{3+} ion. On the other hand, the narrow absorption bands arising from the $^7F_0 \rightarrow {}^{2S+1}L_J$ transitions of Eu^{3+} ion are absent in the excitation spectra presented in Fig. 5, indicating than non-radiative energy transfer from Eu^{3+} to Tb^{3+} ion is not an operative process. As well known, the $^5D_0$ excited level of the Eu^{3+} presents lower energy than the $^5D_4$ acceptor excited level of the Tb^{3+} ion [45,46]. Therefore, the efficient absorption by the $[WO_4]^{2-}$ tungstate group, non-radiative energy transfer and emission by the metal ion, thus overcoming the typically very small absorption coefficients of the RE^{3+} ions. This optical feature makes the rare earth ions an excellent activator for diverse applications in photonic area.

The emission spectra of the $CaWO_4$:Tb^{3+},Eu^{3+},Dy^{3+} (x mol%; x: 0.5–5.0) materials were recorded at room temperature in the range of 420–725 nm under excitation centered on narrow absorption bands at 378 nm assigned to the $^7F_6 \rightarrow {}^5D_3$,$^5G_6$ transitions of Tb^{3+} ion (Fig. 6). These emission spectra show only narrow emission bands arising from the doping Tb^{3+}, Dy^{3+} and Eu^{3+} ions. These emission bands are assigned to the 4f transitions from the $^4F_{9/2}$ (Dy^{3+}), $^5D_4$ (Tb^{3+}) and $^5D_0$ (Eu^{3+}) emitting states to their energy levels corresponding to (in cm^{-1}): 14,238 $^5D_0 \rightarrow {}^7F_4$($Eu^{3+}$), 15,267 $^5D_0 \rightarrow {}^7F_3$($Eu^{3+}$), 16,260 $^5D_0 \rightarrow {}^7F_2$($Eu^{3+}$), 16,886 $^5D_0 \rightarrow {}^7F_1$($Eu^{3+}$), 17,391 $^4F_{9/2} \rightarrow {}^6H_{13/2}$($Dy^{3+}$), 18,362 $^5D_4 \rightarrow {}^7F_5$($Tb^{3+}$), 20,450 $^5D_4 \rightarrow {}^7F_6$($Tb^{3+}$), 20,920 $^4F_{9/2} \rightarrow {}^6H_{15/2}$($Dy^{3+}$).

The presence of the emission bands assigned to the doping dysprosium, terbium and europium ions, with excitation in 378 nm $^7F_6 \rightarrow {}^5D_3$,$^5G_6$ (Tb^{3+}), suggests clear evidence of non-radiative energy transfer from $^4F_{9/2}$ (Dy^{3+})→$^5D_4$ (Tb^{3+})→$^5D_0$ (Eu^{3+}) emitter states (Fig. 7). This energy transfer process is due to the energy level structure of these rare earth ions present their emitter levels very close, only by a few hundred cm^{-1} (Fig. 7). Since the Eu^{3+} can be excited through Tb^{3+} excitation, it is possible consider that there exists an overlapping between terbium $^5D_4 \rightarrow {}^7F_5$, $^5D_4 \rightarrow {}^7F_4$ emissions and europium $^7F_1 \rightarrow {}^5D_1$, $^7F_{0,1} \rightarrow {}^5D_0$ absorptions, respectively. In addition, the more prominent emissions band at around 16,260 cm^{-1} assigned to the rigorously forbidden electric dipole $^5D_0 \rightarrow {}^7F_2$ hypersensitive transition as compared with the intensity of the $^5D_0 \rightarrow {}^7F_1$ transition at 16,886 cm^{-1} which is allowed by magnetic dipole mechanism. This spectroscopic feature suggests that the Eu^{3+} ion is in a chemical environment without center of symmetry. Indeed, $^5D_0 \rightarrow {}^7F_2$ transition is allowed by forced electric dipole and dynamic coupling mechanisms.

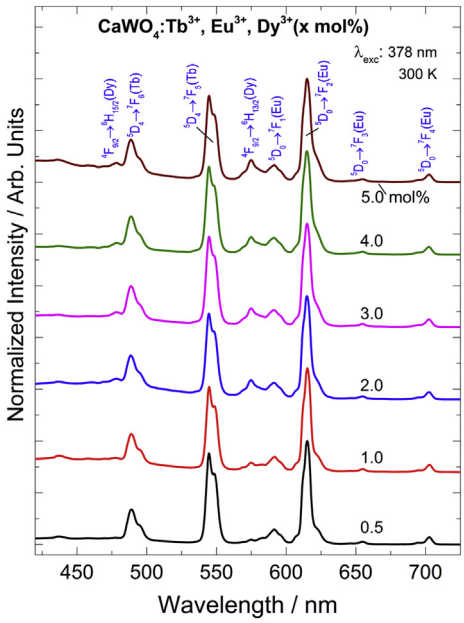

Fig. 6. The emission spectra of the $CaWO_4$:xTb^{3+},xEu^{3+},xDy^{3+} (x: 0.5, 1.0, 2.0, 3.0, 4.0 and 5.0 mol%) materials recorded at room temperature, with UV excitation at 378 nm.

Besides, when the concentration of RE^{3+} ions increase from 0.5 to 5.0 mol% (Fig. 6) it is observed an increasing in relative emission intensities of the $^4F_{9/2} \rightarrow {}^6H_{13/2}$ and $^4F_{9/2} \rightarrow {}^6H_{15/2}$ transitions of the Dy^{3+} ion due to a lower non-radiative energy transfer with an increasing concentration [47–49].

Interestingly, when materials are excited in the $^7F_0 \rightarrow {}^5L_6$ transition of the Eu^{3+} ion at 393 nm the emission spectra show an intensity increasing of the $^5D_0 \rightarrow {}^7F_2$ hypersensitive transition with concentration from 0.5 to 5.0 mol% compared to the 4f transitions of terbium and dysprosium ion. This result suggests that the energy transfer process from $Dy^{3+} \rightarrow Tb^{3+} \rightarrow Eu^{3+}$ become more efficient with the increase of doping concentration leading to higher red color emission.

The lifetime values τ (ms) were obtained from the luminescence decay curves of $CaWO_4$:Eu^{3+},Tb^{3+},Dy^{3+} materials recorded under different excitation wavelengths. The τ values of the materials (Table 1) recorded under excitation at the $^7F_6 \rightarrow {}^5D_3$,$^5G_6$ (~378 nm) transitions and emissions at the $^5D_4 \rightarrow {}^7F_5$ (545 nm) transition of the Tb^{3+} ion decrease from 0.865 to 0.684 ms according to the rare earth ion doping concentration increasing from 0.5 to 4.0 mol% (Fig. 8). This result confirms that the cross-relaxation process is operative, except to the lifetime value of 0.731 ms for the highest concentration (5.0 mol%), suggesting that energy migration between the RE^{3+} ions becomes dominant, with respect to the cross-relaxation process, in these luminescent materials [50,51].

The coordinates in the CIE (*Commission Internationale l'Éclairage*) chromaticity diagram of the of $CaWO_4$:Tb^{3+},Eu^{3+},Dy^{3+}

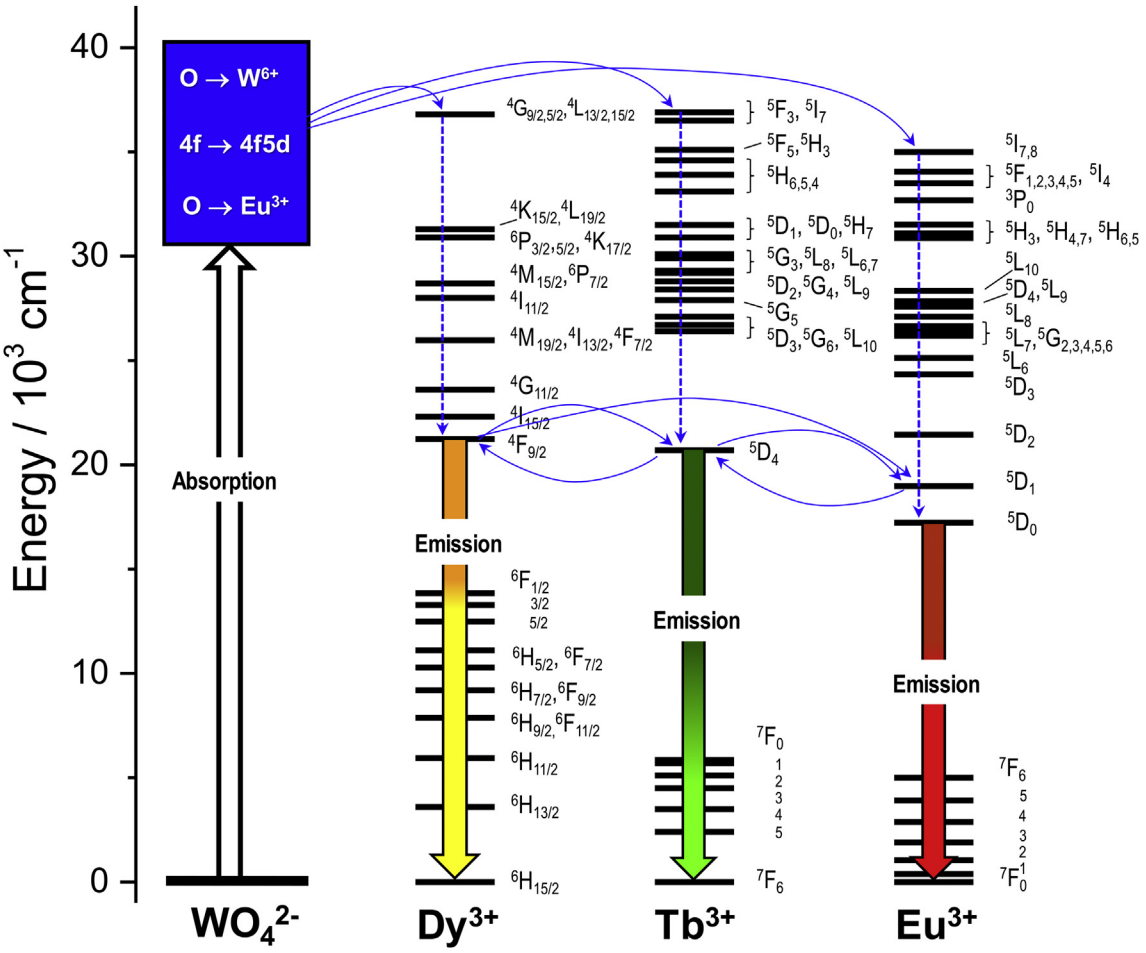

Fig. 7. Partial energy level diagram of $CaWO_4$:Tb^{3+},Eu^{3+},Dy^{3+} materials presenting the transitions involved in the energy transfers (curve arrows), non-radiative decays (dashed arrows) WO_4^{2-} → RE^{3+}, Dy^{3+}→Tb^{3+}, Dy^{3+}→Eu^{3+} and Tb^{3+}→Eu^{3+}, as well as their simultaneous emission [41,44].

Table 1
Lifetimes values (τ, ms) obtained at different excitation wavelength for the Eu^{3+}, Tb^{3+} and Dy^{3+} ions and CIE chromaticity parameters and color correlated temperature (CCT) values of the $CaWO_4$:xTb^{3+},xEu^{3+},xDy^{3+} (x: 0.5–5.0 mol%) materials.

$CaWO_4$:xTb^{3+},xEu^{3+},xDy^{3+}	Lifetimes (ms)			CIE	CCT
(x mol%)	[a]Tb^{3+}	[b]Eu^{3+}	[c]Dy^{3+}	(x; y)	(K)
0.5	0.865	0.715	0.333	0.377; 0.414	4308
1.0	0.834	0.686	0.312	0.335; 0.372	5411
2.0	0.707	0.584	0.289	0.321; 0.373	5933
3.0	0.687	0.583	0.262	0.355; 0.392	4802
4.0	0.684	0.578	0.263	0.380; 0.406	4195
5.0	0.731	0.628	0.265	0.333; 0.352	5479

[a] Tb^{3+}: $\lambda_{exc.}$ = 378 nm; $\lambda_{em.}$ = 545 nm.
[b] Eu^{3+}: $\lambda_{exc.}$ = 393 nm; $\lambda_{em.}$ = 614 nm.
[c] Dy^{3+}: $\lambda_{exc.}$ = 385 nm; $\lambda_{em.}$ = 576 nm.

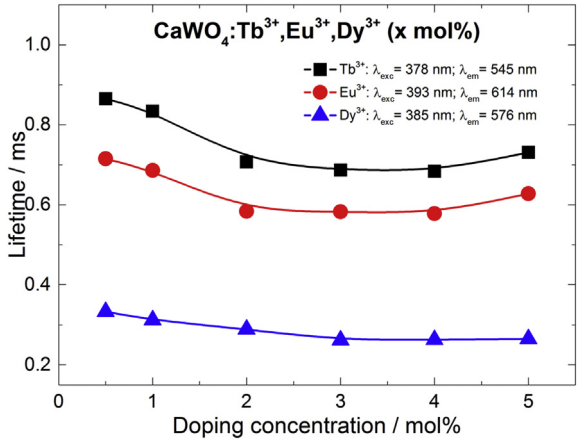

Fig. 8. Lifetimes values of $CaWO_4$:xTb^{3+},xEu^{3+},xDy^{3+} (x: 0.5–5.0 mol%) phosphors as a function of RE^{3+} concentrations, under excitation and monitoring emission in the Tb^{3+}, Eu^{3+} and Dy^{3+} ions.

suggests that the doping materials exhibit whitish emissions colors when doping concentrations 0.5, 1.0, 2.0, 3.0, 4.0 and 5.0 mol%, under excitation at 378 nm corresponding to the $^7F_6$→$^5G_6$ (Tb^{3+}) transition (Fig. 9) [35]. The color correlated temperature (CCT) values (summarized in Table 1) were calculated by the following Equation (2): [7,52].

$$\mathbf{CCT} = -449\mathbf{n}^3 + 3525\mathbf{n}^2 - 6823.3\mathbf{n} + 5520.33 \quad (2)$$

where $n = (x - x_e)/(y - y_e)$ is the reciprocal slope and x_e: 0.3320; y_e: 0.1858 is the chromaticity epicenter. The CCT values of 4308; 5411; 5933; 4802; 4195 and 5479 K are assigned to the 0.5, 1.0, 2.0, 3.0, 4.0 and 5.0 mol% doping concentration of RE^{3+}, respectively (Table 1). The white light emission was mainly reached for 5.0 mol% RE^{3+} with x: 0.333; y: 0.352 CIE coordinates.

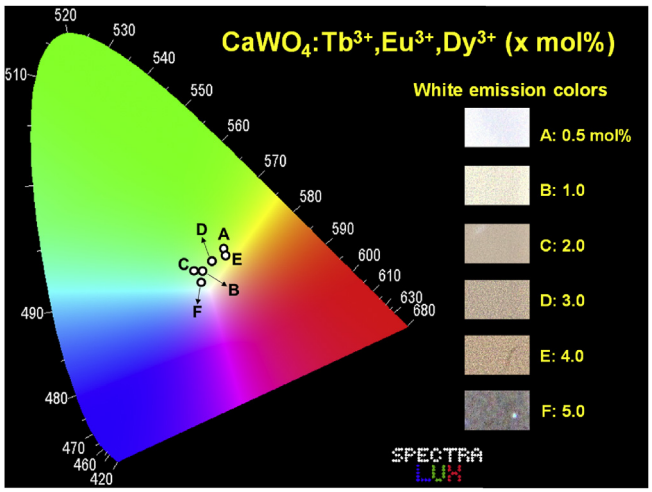

Fig. 9. The CIE chromatic diagram showing the coordinates for the $CaWO_4:Eu^{3+},Tb^{3+},Dy^{3+}$; x: 0.5–5.0 mol%). The figures are photographs of the luminescent materials taken with a digital camera displaying the whitish emissions, under UV irradiation at 378 nm.

The presence of the Tb^{3+}, Eu^{3+} and Dy^{3+} ions and tungstate host lattice provide different excitation wavelengths due to $O^{2-}(2p)\rightarrow Eu^{3+}(4f)$, $O^{2-}(2p)\rightarrow W^{VI}(5d)$ Ligand–to–Metal Charge Transfer (LMCT) states and Tb^{3+} $4f^8\rightarrow 4f^75d^1$ interconfigurational as well as 4f-4f transitions, leading to white light emission tunable levels of chromaticity. Moreover, the doped materials were excited at 260, 378 and 393 nm, yielding to tuning of emission colors between cool and warm white light (Figs. S2 and S3 and S4). Since warm white light is preferred for reading, while cold white light is preferred for public lighting the tunability of this single-phase emitting phosphors exhibit promising applications for solid-state lighting [53].

5. Conclusion

The triply-doped $CaWO_4:xTb^{3+},xEu^{3+},xDy^{3+}$ (x mol%; x: 0.5–5.0) materials were successfully prepared by the coprecipitation method at room temperature. The synthesis was carried out under aqueous condition without the use of any catalyst, organic solvent or surfactant. Furthermore, the crystallite sizes of the doped materials are at around 11 nm. The phosphors with different RE^{3+} concentrations (RE^{3+}: Tb, Eu and Dy) between 0.5 and 5.0 mol% for each activator ion exhibited their characteristic excitation and emission transitions, leading to white light emission under UV excitation.

The non-radiative energy transfer occurs via higher energy levels from the O→W and O→Eu LMCT states as well as the $4f^8\rightarrow 4f^75d^1$ transitions to intraconfigurational 4f transitions of rare earth ions and mainly arises from the $^4F_{9/2}$ (Dy^{3+})→$^5D_4$ (Tb^{3+})→$^5D_1$, $^5D_0$ (Eu^{3+}) emitter levels which are very close (or in resonance) in energies. In addition, the energy transfer process between emitter levels from the Dy^{3+} to Eu^{3+} ions is also operative. With the increasing of RE^{3+} ions concentration (in the range 0.5–5.0 mol%) the color changes gradually and has contribution from near whitish blue to warm white. Meanwhile, the CCT values of the prepared phosphors were also varied and the emission color was tuned from cool white (5479 K) to warm white (4308 K). These phosphors could be suitable as triply-doped white light emitters with only single-phased for solid state lighting applications.

Acknowledgements

The authors thank the following Brazilian agencies for financial support: Conselho Nacional de Desenvolvimento Científico e Tecnológico (407820/2013-2), the Coordenação de Aperfeiçoamento de Pessoal de Nível Superior (Programa Rede-Nanobiotec-Brasil Edital Rede Nanobiotec-Brasil N. 04/2008) and the Fundação de Amparo à Pesquisa do Estado de São Paulo (15/15045-5), as well as the photographer Cezar Guizzo.

Appendix A. Supplementary data

Supplementary data related to this article can be found at http://dx.doi.org/10.1016/j.jallcom.2016.11.378.

References

[1] P.F. Smet, A.B. Parmentier, D. Poelman, Selecting conversion phosphors for white light-emitting diodes, J. Electrochem. Soc. 158 (2011) R37–R54, http://dx.doi.org/10.1149/1.3568524.
[2] Z. Luo, G. Qi, K. Chen, M. Zou, L. Yuwen, X. Zhang, W. Huang, L. Wang, Microwave-Assisted preparation of white fluorescent graphene quantum dots as a novel phosphor for enhanced white-light-emitting diodes, Adv. Funct. Mater. 26 (2016) 2739–2744, http://dx.doi.org/10.1002/adfm.201505044.
[3] B. Wang, H. Lin, J. Xu, H. Chen, Y. Wang, $CaMg_2Al_{16}O_{27}:Mn^{4+}$-based red phosphor: a potential color converter for high-powered warm W-LED, ACS Appl. Mater. Interfaces 6 (2014) 22905–22913, http://dx.doi.org/10.1021/am507316b.
[4] W. Ma, Z. Shi, R. Wang, Luminescence properties of full-color single-phased phosphors for white LEDs, J. Alloys Compd. 503 (2010) 118–121, http://dx.doi.org/10.1016/j.jallcom.2010.04.213.
[5] X. Ding, G. Zhu, W. Geng, Q. Wang, Y. Wang, Rare-earth-free high-efficiency narrow-band red-emitting $Mg_3Ga_2GeO_8:Mn^{4+}$ phosphor excited by near-UV light for white-light-emitting diodes, Inorg. Chem. 55 (2016) 154–162, http://dx.doi.org/10.1021/acs.inorgchem.5b02048.
[6] P. Du, J.S. Yu, Energy transfer mechanism and color controllable luminescence in Dy^{3+}/Eu^{3+}-codoped $NaLa(MoO_4)_2$ phosphors, J. Alloys Compd. 653 (2015) 468–473, http://dx.doi.org/10.1016/j.jallcom.2015.08.256.
[7] S. Som, P. Mitra, V. Kumar, V. Kumar, J.J. Terblans, H.C. Swart, S.K. Sharma, The energy transfer phenomena and colour tunability in Y_2O_2S: Eu^{3+}/Dy^{3+} microfibers for white emission in solid state lighting applications, Dalton Trans. 43 (2014) 9860–9871, http://dx.doi.org/10.1039/c4dt00349g.
[8] L. Wu, Y. Zhang, M. Gui, P. Lu, L. Zhao, S. Tian, Y. Kong, J. Xu, Luminescence and energy transfer of a color tunable phosphor: Dy3+-, Tm3+-, and Eu3+-coactivated KSr4(BO3)3 for warm white UV LEDs, J. Mater. Chem. 22 (2012) 6463–6470, http://dx.doi.org/10.1039/c2jm15506k.
[9] Y. Zhu, Y. Liang, M. Zhang, M. Tong, G. Li, S. Wang, Structure, luminescence properties and energy transfer behavior of color-adjustable $Sr_3Gd_2(Si_3O_9)_2$: $Ce^{3+},Tb^{3+}/Mn^{2+}$ phosphors, RSC Adv. 5 (2015) 98350–98360, http://dx.doi.org/10.1039/C5RA20756H.
[10] K. Li, D. Geng, M. Shang, Y. Zhang, H. Lian, J. Lin, Color-tunable luminescence and energy transfer properties of $Ca_9Mg(PO_4)_6F_2:Eu^{2+},Mn^{2+}$ phosphors for UV-LEDs, J. Phys. Chem. C 118 (2014) 11026–11034, http://dx.doi.org/10.1021/jp501949m.
[11] J. Sun, Z. Lian, G. Shen, D. Shen, Blue–white–orange color-tunable luminescence of Ce^{3+}/Mn^{2+}-codoped $NaCaBO_3$ via energy transfer: potential single-phase white-light-emitting phosphors, RSC Adv. 3 (2013) 18395–18405, http://dx.doi.org/10.1039/c3ra42554a.
[12] Z. Mao, Y. Zhu, Y. Wang, L. Gan, Ca_2SiO_4:Ln (Ln = Ce^{3+}, Eu^{2+}, Sm^{3+}) tricolor emission phosphors and their application for near-UV white light-emitting diode, J. Mater. Sci. 49 (2014) 4439–4444, http://dx.doi.org/10.1007/s10853-014-8140-4.
[13] B. Yuan, Y. Sheng, Y. Song, K. Zheng, X. Zhou, X. Xu, H. Zou, Luminescent properties of $Ca_2Mg_{0.75}Al_{0.5}Si_{1.75}O_7$:Ln (Ln=$Ce^{3+}$, Dy^{3+}, Eu^{3+}, Sm^{3+}) and their application for UV white light-emitting diodes, J. Alloys Compd. 644 (2015) 82–90, http://dx.doi.org/10.1016/j.jallcom.2015.04.192.
[14] A. Poddar, S.C. Gedam, S.J. Dhoble, Synthesis of $KMgCl_3$ nanomaterial and luminescence of $Ce^{3+}/Dy^{3+}/Eu^{3+}$ by different routes, J. Lumin. 158 (2015) 188–196, http://dx.doi.org/10.1016/j.jlumin.2014.09.049.
[15] W. Bolaños, J.J. Carvajal, X. Mateos, M.C. Pujol, N. Thilmann, V. Pasiskevicius, G. Lifante, M. Aguiló, F. Díaz, Epitaxial layers of $KY_{1-x-y}Gd_xLu_y(WO_4)_2$ doped with Er^{3+} and Tm^{3+} for planar waveguide lasers, Opt. Mater. 32 (2010) 469–474, http://dx.doi.org/10.1016/j.optmat.2009.10.011.
[16] T. Thongtem, S. Kungwankunakorn, B. Kuntalue, A. Phuruangrat, S. Thongtem, Luminescence and absorbance of highly crystalline $CaMoO_4$, $SrMoO_4$, $CaWO_4$ and $SrWO_4$ nanoparticles synthesized by co-precipitation method at room temperature, J. Alloys Compd. 506 (2010) 475–481, http://dx.doi.org/10.1016/j.jallcom.2010.07.033.
[17] J. Kido, Y. Okamoto, Organo lanthanide metal complexes for electroluminescent materials, Chem. Rev. 102 (2002) 2357–2368, http://dx.doi.org/10.1021/cr010448y.
[18] L.D. Carlos, R.A.S. Ferreira, V.D.Z. Bermudez, S.J.L. Ribeiro, Lanthanide-containing light-emitting organic-inorganic hybrids: a bet on the future, Adv.

Mater. 21 (2009) 509–534, http://dx.doi.org/10.1002/adma.200801635.
[19] G.-H. Lee, S. Kang, Solid-solution red phosphors for white LEDs, J. Lumin. 131 (2011) 2582–2588, http://dx.doi.org/10.1016/j.jlumin.2011.06.025.
[20] F.B. Xiong, H.F. Lin, L.J. Wang, X.G. Meng, W.Z. Zhu, White light emission in host-sensitized Dy^{3+}-single-doped $NaIn(WO_4)_2$ phosphors, Phys. B Condens. Matter. 459 (2015) 41–45, http://dx.doi.org/10.1016/j.physb.2014.11.100.
[21] Y. Tian, B. Chen, R. Hua, N. Yu, B. Liu, J. Sun, L. Cheng, H.H. Zhong, X. Li, J. Zhang, B. Tian, H.H. Zhong, Self-assembled 3D flower-shaped $NaY(WO_4)_2$:Eu^{3+} microarchitectures: microwave-assisted hydrothermal synthesis, growth mechanism and luminescent properties, CrystEngComm 14 (2012) 1760–1769, http://dx.doi.org/10.1039/c1ce06232h.
[22] H.P. Barbosa, J. Kai, I.G.N. Silva, L.C.V. Rodrigues, M.C.F.C. Felinto, J. Hölsä, O.L. Malta, H.F. Brito, Luminescence investigation of R^{3+}-doped alkaline earth tungstates prepared by a soft chemistry method, J. Lumin. 170 (2016) 736–742, http://dx.doi.org/10.1016/j.jlumin.2015.07.014.
[23] K. Zheng, Z. Liu, C. Lv, W. Qin, Temperature sensor based on the UV upconversion luminescence of Gd^{3+} in Yb^{3+}–Tm^{3+}–Gd^{3+} codoped $NaLuF_4$ microcrystals, J. Mater. Chem. C 1 (2013) 5502, http://dx.doi.org/10.1039/c3tc30763h.
[24] V. Kumar Rai, A. Pandey, R. Dey, Photoluminescence study of Y_2O_3:Er^{3+}-Eu^{3+}-Yb^{3+} phosphor for lighting and sensing applications, J. Appl. Phys. 113 (2013) 83104, http://dx.doi.org/10.1063/1.4793265.
[25] J. Zhang, S. Wang, T. Rong, L. Chen, Upconversion luminescence in Er^{3+} doped and Yb^{3+}/Er^{3+} codoped yttria nanocrystalline powders, J. Am. Ceram. Soc. 87 (2004) 1072–1075. http://onlinelibrary.wiley.com/doi/10.1111/j.1551-2916.2004.01072.x/abstract.
[26] B.-I. Lee, E. Lee, S.-H. Byeon, Assembly of layered rare-earth hydroxide nanosheets and SiO_2 nanoparticles to fabricate multifunctional transparent films capable of combinatorial color generation, Adv. Funct. Mater. 22 (2012) 3562–3569, http://dx.doi.org/10.1002/adfm.201200295.
[27] R.A. Hewes, Multiphoton excitation and efficiency in the Yb^{3+}-$R.E.^{3+}$ (Ho^{3+}, Er^{3+}, Tm^{3+}) systems, J. Lumin. 1–2 (1970) 778–796, http://dx.doi.org/10.1016/0022-2313(70)90090-6.
[28] H. Sun, D. Peng, X. Wang, M. Tang, Q. Zhang, X. Yao, Green and red emission for $(K_{0.5}Na_{0.5})NbO_3$:Pr ceramics, J. Appl. Phys. 111 (2012) 46102, http://dx.doi.org/10.1063/1.3686193.
[29] A.K. Soni, R. Dey, V.K. Rai, Stark sublevels in Tm^{3+}-Yb^{3+} codoped $Na_2Y_2B_2O_7$ nanophosphor for multifunctional applications, Rsc Adv. 5 (2015) 34999–35009, http://dx.doi.org/10.1039/c4ra15891a.
[30] J. Pisarska, A. Kos, W.A. Pisarski, Spectroscopy and energy transfer in lead borate glasses doubly doped with Dy^{3+}–Tb^{3+} and Tb^{3+}–Eu^{3+} ions, Spectrochim. Acta Part A Mol. Biomol. Spectrosc. 129 (2014) 649–653, http://dx.doi.org/10.1016/j.saa.2014.04.142.
[31] J. Pisarska, A. Kos, E. Pietrasik, W.A. Pisarski, Energy transfer from Dy^{3+} to Tb^{3+} in lead borate glass, Mater. Lett. 129 (2014) 146–148, http://dx.doi.org/10.1016/j.matlet.2014.05.035.
[32] A. Khanna, P.S. Dutta, Narrow spectral emission $CaMoO_4$: Eu^{3+},Dy^{3+},Tb^{3+} phosphor crystals for white light emitting diodes, J. Solid State Chem. 198 (2013) 93–100, http://dx.doi.org/10.1016/j.jssc.2012.08.060.
[33] A.M. Kaczmarek, R. Van Deun, Rare earth tungstate and molybdate compounds - from 0D to 3D architectures, Chem. Soc. Rev. 42 (2013) 8835–8848, http://dx.doi.org/10.1039/c3cs60166h.
[34] Q. Zhang, Q. Meng, W. Sun, The concentration dependence of luminescent properties for Eu^{3+} doped $CaWO_4$ micron spherical phosphors, Opt. Mater. 35 (2013) 915–922, http://dx.doi.org/10.1016/j.optmat.2012.11.012.
[35] P.A. Santa-Cruz, F.S. Teles, Spectra lux software v.2.0 beta, ponto quântico nanodispositivos, RENAMI (2003).
[36] X. Li, J. Li, Q. Zhou, Z. Peng, G. Liu, T. Qi, Direct hydrothermal precipitation of pyrochlore-type tungsten trioxide hemihydrate from alkaline sodium tungstate solution, Metall. Mater. Trans. B 43 (2012) 221–228, http://dx.doi.org/10.1007/s11663-011-9615-1.
[37] T. Thongtem, A. Phuruangrat, S. Thongtem, Characterization of $MeWO_4$ (Me=Ba, Sr and Ca) nanocrystallines prepared by sonochemical method, Appl. Surf. Sci. 254 (2008) 7581–7585, http://dx.doi.org/10.1016/j.apsusc.2008.01.092.
[38] The International Centre for Diffraction Data – ICDD, Entries 41–1431: $CaWO_4$, 23–525: $Dy_2(WO_4)_3$, 72-0504: $Eu_2(WO_4)_3$ and 28-1290: $Tb_2(WO_4)_3$, 1997.
[39] R.D. Shannon, Revised effective ionic radii and systematic studies of interatomic distances in halides and chalcogenides, Acta Crystallogr. Sect. A. A32 (1976) 751–767, http://dx.doi.org/10.1107/S0567739476001551.
[40] E. Cavalli, P. Boutinaud, R. Mahiou, M. Bettinelli, P. Dorenbos, Luminescence dynamics in Tb^{3+}-doped $CaWO_4$ and $CaMoO_4$ crystals, Inorg. Chem. 49 (2010) 4916–4921, http://dx.doi.org/10.1021/ic902445c.
[41] H.P. Klug, L.E. Alexander, X-Ray Diffraction Procedures, 1959. New York.
[42] Y. Gao, Y. Sun, H. Zou, Y. Sheng, X. Zhou, B. Zhang, B. Zhou, Effect of Eu^{3+} doping on the structural and photoluminescence properties of cubic $CaCO_3$, Mater. Sci. Eng. B 203 (2016) 52–58, http://dx.doi.org/10.1016/j.mseb.2015.09.004.
[43] C.A. Kodaira, H.F. Brito, O.L. Malta, O.A. Serra, Luminescence and energy transfer of the europium (III) tungstate obtained via the Pechini method, J. Lumin. 101 (2003) 11–21, http://dx.doi.org/10.1016/S0022-2313(02)00384-8.
[44] W.T. Carnall, G.L. Goodman, K. Rajnak, R.S. Rana, A systematic analysis of the spectra of the lanthanides doped into single crystal LaF_3, J. Chem. Phys. 90 (1989) 3443–3457, http://dx.doi.org/10.1063/1.455853.
[45] H.F. Brito, O.L. Malta, M.C.F.C. Felinto, E.E.S. Teotonio, Luminescence Phenomena Involving Metal Enolates, John Wiley & Sons, Ltd, Chichester, UK, 2009, http://dx.doi.org/10.1002/9780470682531.pat0419.
[46] C.C.S. Pedroso, J.M. Carvalho, L.C.V. Rodrigues, J. Hölsä, H.F. Brito, Rapid and Energy-Saving Microwave-Assisted Solid-state synthesis of Pr^{3+}-, Eu^{3+}-, or Tb^{3+}-Doped Lu_2O_3 persistent luminescence materials, ACS Appl. Mater. Interfaces 8 (2016) 19593–19604, http://dx.doi.org/10.1021/acsami.6b04683.
[47] X. Xiao, B. Yan, Chemical co-precipitation synthesis and photoluminescence of Eu^{3+} or Dy^{3+} doped $Zn_3Nb_2O_8$ microcrystalline phosphors from hybrid precursors, Mater. Sci. Eng. B 136 (2007) 154–158, http://dx.doi.org/10.1016/j.mseb.2006.09.020.
[48] D. Gao, Y. Li, X. Lai, Y. Wei, J. Bi, Y. Li, M. Liu, Fabrication and luminescence properties of Dy^{3+} doped $CaMoO_4$ powders, Mater. Chem. Phys. 126 (2011) 391–397, http://dx.doi.org/10.1016/j.matchemphys.2010.10.053.
[49] X. Zhang, F. Meng, W. Li, S. Il Kim, Y.M. Yu, H.J. Seo, Investigation of energy transfer and concentration quenching of Dy^{3+} luminescence in $Gd(BO_2)_3$ by means of fluorescence dynamics, J. Alloys Compd. 578 (2013) 72–76, http://dx.doi.org/10.1016/j.jallcom.2013.05.012.
[50] A.N. Meza-Rocha, R. Lozada-Morales, A. Speghini, M. Bettinelli, U. Caldiño, White light generation in Tb^{3+}/Eu^{3+}/Dy^{3+} triply-doped $Zn(PO_3)_2$ glass, Opt. Mater. (Amst) 51 (2016) 128–132, http://dx.doi.org/10.1016/j.optmat.2015.11.032.
[51] L. Li, R. Li, W. Zi, S. Gan, Hydrothermal synthesis and luminescent properties of color-tunable Dy^{3+} doped and Eu^{3+}/Tb^{3+} co-doped $MMoO_4$ (M=Ca, Sr, Ba) phosphors, Phys. B Condens. Matter. 458 (2015) 8–17, http://dx.doi.org/10.1016/j.physb.2014.11.001.
[52] C.S. McCamy, Correlated color temperature as an explicit function of chromaticity coordinates, Color Res. Appl. 17 (1992) 142–144, http://dx.doi.org/10.1002/col.5080170211.
[53] G. Lakshminarayana, R. Yang, J.R. Qiu, M.G. Brik, G.A. Kumar, I.V. Kityk, White light emission from Sm^{3+}/Tb^{3+} codoped oxyfluoride aluminosilicate glasses under UV light excitation, J. Phys. D. Appl. Phys. 42 (2009) 15414, http://dx.doi.org/10.1088/0022-3727/42/1/015414.